Lasers in Manufacturing Conference 2021

Experimental and numerical analysis of local gas supplies for spatter reduced high speed laser beam welding

Leander Schmidt[a,*], Klaus Schricker[a], Jean Pierre Bergmann[a]

[a]*Technische Universität Ilmenau, Production Technology Group, Gustav-Kirchhoff-Platz 2, 98693 Ilmenau, Germany*

Abstract

Spatter formation is a major issue in deep penetration welding with solid-state lasers at high welding speeds. The use of local gas supplied near to the keyhole proved to be very effective to avoid spatter formation. This publication examines the flow conditions and pressure field of a local supply of argon/helium by welding stainless steel (X5CrNi18-10/AISI304) at welding speeds beyond 8 m/min to get a deeper understanding of the acting mechanisms. By varying the flow rate, the flow field characteristics were visualized by Schlieren imaging and quantified by Schlieren image velocimetry (flow pattern, flow velocity). In order to specify the resulting pressure field, a computational fluid dynamics analysis have been performed based on a k-ω-SST multi component turbulence model. By combining the experimental und numerical findings, it was possible to derive a comprehensive model representation of the fundamental effect mechanisms.

Keywords: welding; macro processing; spatter formation; low-spatter welding; effect of local gas supply

1. Introduction

The use of a local gas flow supplied near keyhole aperture has proven to be very effective in limiting keyhole instabilities and spatter formation during deep penetration laser beam welding. In this context, Kamikuki et al., 2002 demonstrated a significant effect of a lateral gas flow of argon at deep penetration laser beam welding of high-alloy steel AISI304 (X5CrNi18-10, 1.4301) at a welding speed of 1 m/min by reducing pores and spatter formation. A follow-up study of Fabbro et al., 2006 gained comparable results for welding speeds up to 5 m/min. In both studies, the gas flow led to an enlargement of the keyhole aperture. The affected outgassing conditions of the metal vapor flow has been stated as the acting main mechanism. Investigations

* Corresponding author.
E-mail address: leander.schmidt@tu-ilmenau.de .

of Jovic et al., 2019 and Jovic et al., 2020 also demonstrated a stabilizing effect of the gas flow on the keyhole formation and a reduction in spatter formation for welding of martensitic steel in lap joints at a welding speed of 1.5 m/min. Depending on flow rate, a bulging of the keyhole rear wall was observed. Further studies of Schmidt et al., 2019 and Schmidt et al., 2020 for partial and full penetration welding of high-alloy-steel AISI304 (X5CrNi18-10, 1.4301) at high welding speeds from 8 m/min to 16 m/min underline the positive effect of the gas flow on keyhole stability and spatter formation. The effect of the gas flow was primarily attributed to the additional applied pressure term p_{gas} on the general pressure balance of the keyhole in these cases. According to Beck, 1996 and Katayama et al., 2013, the pressure balance significantly affects keyhole stability and describes the relation between opening and closing pressures of the keyhole (equation 1).

$$p_{recoil} + \Delta p_{dp\_v} + p_{gas} = p_\sigma + p_h + p_{dyn};\ \Delta p_{dp\_v} = p_v - p_0 \tag{1}$$

The physical quantities are p_{recoil} as recoil pressure, Δp_{dp_v} as differential vapor pressure, p_σ as surface tension pressure, p_h as hydrostatic pressure, p_{dyn} as hydrodynamic pressure, p_v as vapor pressure and p_0 as atmospheric pressure. In order to represent the effect of the gas supply in a more comprehensive form, the magnitude of the pressure term p_{gas} can be approximated in terms of the dynamic pressure of the gas p_{dyn_gas} (equation 2).

$$p_{dyn\_gas} = \frac{1}{2} \cdot \rho_{gas} \cdot v_{gas}^2 \tag{2}$$

The physical quantities are ρ_{gas} as gas density and v_{gas} as flow velocity of the gas.

To determine the influence of the affected pressure balance on keyhole stability and melt pool dynamics in more detail, various investigations were carried out using computational fluid dynamics (CFD). According to the first experimental results of Kamikuki et al., 2002, which demonstrated a reduction in fluctuations of the keyhole real wall, Amara et al., 2008 could achieve comparable results by CFD analysis. In addition, it was found that the use of the gas flow reduces recirculation in the rear-sided melt pool, which leads to a significant melt pool elongation due to a more uniform melt propagation. Further, Zhang et al., 2011 determined an acceleration of near-surface melt against welding direction while using trailing and central orientated gas supplies. In addition, he could also observe a stabilization of the keyhole real wall, which resulted in a decreasing spatter and pore formation. Wu et al., 2018 could figure out, that a leading flow orientation has a destabilizing effect on the keyhole during deep penetration welding of aluminum AA 5083. In this context, he attributed the phenomenon to an increased upward momentum of the molten material.

However, despite the numerous studies concerning the effect of gas flow on melt pool dynamics and keyhole formation, a specific analysis of the inflow characteristics and resulting pressure distribution of the gas flow is currently incomplete. Therefore, this publication examines the experimental and analytical characterization of the pressure field and resulting flow field characteristics of a local gas supply of helium by a follow-up study of Schmidt et al., 2019. Schlieren videography and computational fluid dynamics analysis have been used to link previous findings on keyhole stability to the applied pressure distribution and flow field characteristics (flow pattern, flow velocity) of a local gas supply.

2. Materials and methods

2.1. Experimental setup

The experimental setup is based on Schmidt et al., 2019 respectively Schmidt et al., 2020 and has been adapted for Schlieren videography of the local gas supply. To get a deeper understanding of the general effects,

the experimental procedure was carried out while the laser power was deactivated to separate the influence of the welding process (e.g., outflowing metal vapor, thermal convection) on the flow field of the supplied gas (Fig. 1 a, b). The same gas nozzle unit was used in a stationary arrangement as in Schmidt et al., 2019 (Fig. 1 c). Based on the parameters for the lowest loss of mass of Schmidt et al., 2019, the nozzle unit was set in a trailing orientation with an angle of incidence of 48 ° by using three linear guidance and one ration axis. The nozzle had an inner diameter of 1.2 mm and was positioned in a distance of 5 mm to specimen surface. Stainless austenitic steel 1.4301 (X5CrNi18-10, AISI 304) in dimensions of 150 mm x 40 mm x 2 mm was used. The resulting flow pattern of the local gas supply was visualized by using an in-house developed Schlieren apparatus (Fig. 1 b), which allows a high-speed recording of the flow pattern based on the difference in density and refractive index between supplied gas and surrounding atmosphere. Further details in Schlieren imaging are given in Settles, 2001. This study focuses on the usage of helium. This can be attributed to the higher difference in density of helium ($\rho_{Hel} \approx 0{,}18\ kg \cdot m^{-1}$) to the surrounding atmosphere ($\rho_{atm} \approx 1{,}20\ kg \cdot m^{-1}$) compared to using argon ($\rho_{Ar} \approx 1{,}78\ kg \cdot m^{-1}$) that allows a high-contrast visualization of the forming flow pattern. When interpreting and comparing the flow field characteristics of this publication to previously investigations using argon, the differences in thermophysical properties of helium and argon should be considered, because the flow conditions of the gas will be affected. The forming flow pattern was recorded by means of a Photron SA-X2 high-speed camera at a frame rate of 10,000 frames per second at a resolution of 1024 px · 1024 px. The captured images were pre-processed by subtracting the moving average of the whole image sequence. Afterwards, the images were binarized to be analyzed using a Matlab-based image plugin for particle image velocimetry (PIVlab) according to Thielicke et al., 2014 and Thielicke, 2014. The PIV-analysis was performed using the time-resolved image import function without any additional image pre-processing. The particle displacement was detected using a fast Fourier transformation window deformation analysis with four interrogation area phases and a 2 x 3-point gauss subpixel estimator, while auto correlation was disabled. Afterwards, the vector fields were filtered using a standard deviation filter to eliminate vector sizes greater than eight times of the standard deviation.

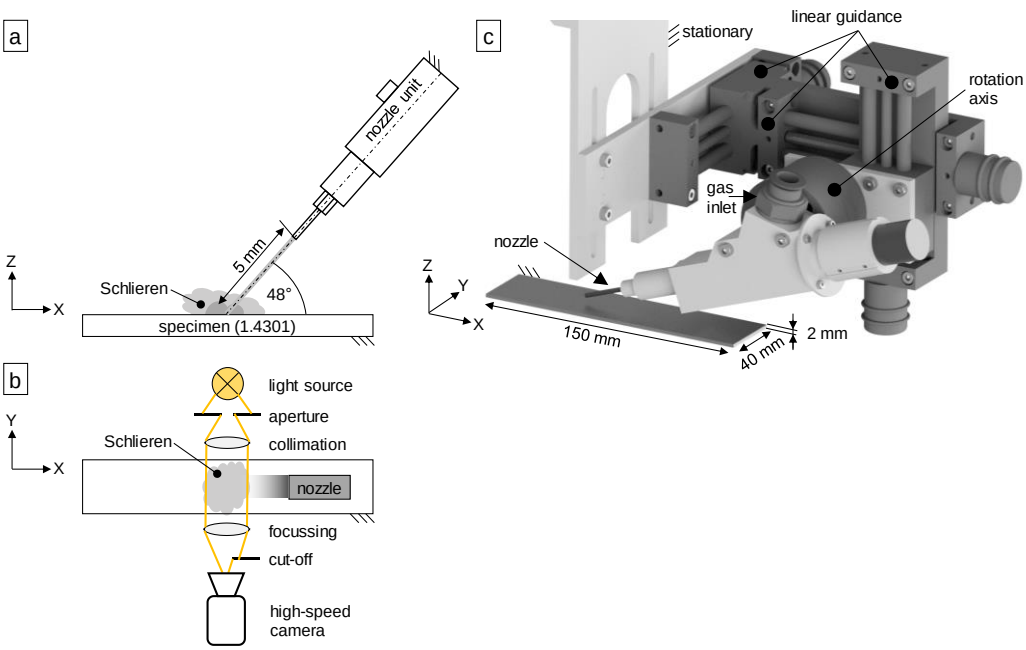

Fig. 1. Schematic experimental setup: (a) X-Z-view; (b) X-Y-view, (c) Specs of used nozzle unit

2.2. Numerical simulation

Comsol Multiphysics 5.6 was used for a simplified numerical simulation of the gas flow supplied by the nozzle. The transient flow field was calculated based on a Shear-Stress-Transport turbulence model (SST) in combination with transport of concentrated species (TCS). SST enables a sufficient simulation of flow processes near and far from a wall (Dreher et al., 2009). TCS was applied in order to model the mixture between gas and surrounding atmosphere based on a mixture-averages diffusion model (see Comsol Multiphysics 5.6, 2021). The linkage of SST and TCS allowed an adequate representation of the flow field.

Considerable simplifications were assumed to minimize computational times, especially the modelling as a 2D flow field based on the central axis of the gas nozzle. In addition, the gases were assumed to be incompressible, gravity acts on entire flow field, turbulent Schmidt number was kept constant for turbulent mixing and the gas inflow was assumed as fully developed. The simulation did not take into account any effects due to the welding process, i.e. the effect of metal vapor or elevated temperatures was not considered. Temperature was kept constant at 20 °C (T_0) and an initial pressure of 1.013 mbar (p_0) was set. The effect of simplifications on numerical results and their validity will be discussed in section 3.

The model concept and the boundary conditions for calculating the resulting flow field are shown in Fig. 2. The inflow velocity v_{in} of helium was calculated based on different volume flows used in the experiment. The gas flowed out perpendicular to the nozzle tip. The angle of the nozzle and the distance to the surface were consistent with the experiment described in section 2.1. The nozzle and the sheet surface were modelled as walls, i.e. no flow across these boundaries is possible with exception of the inflow at the nozzle tip. This is particularly relevant for the area below the nozzle, as the gas could flow upwards around the nozzle in the experiment. However, this effect was neglected due to the simplified 2D simulations. Slip at walls was not considered. The mesh was refined in the areas close to the surface in order to gain sufficient results of the gas flow in those areas. The surrounding outlet allowed a flow of helium and air in both directions with no additional pressure added.

The simulations were evaluated regarding flow field and resulting mixture of both gases at different time steps. Pressure and velocity fields were considered additionally to compare simulations and experiments.

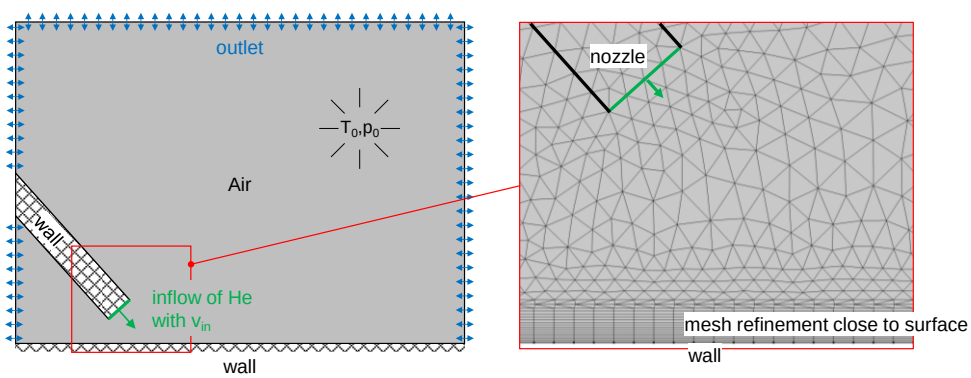

Fig.2. Model concept and boundary conditions

3. Results and discussion

3.1. Effect on melt pool dynamics and spatter formation

This study is based on results of the previous study Schmidt et al., 19, that characterized the effect of a local gas flow of argon on melt pool dynamics and spatter formation. In this context, Fig. 2 provides an overview of the relevant findings by comparing the effect of the gas supply (*Local Gas*) to the reference process without gas supply (*Reference*).

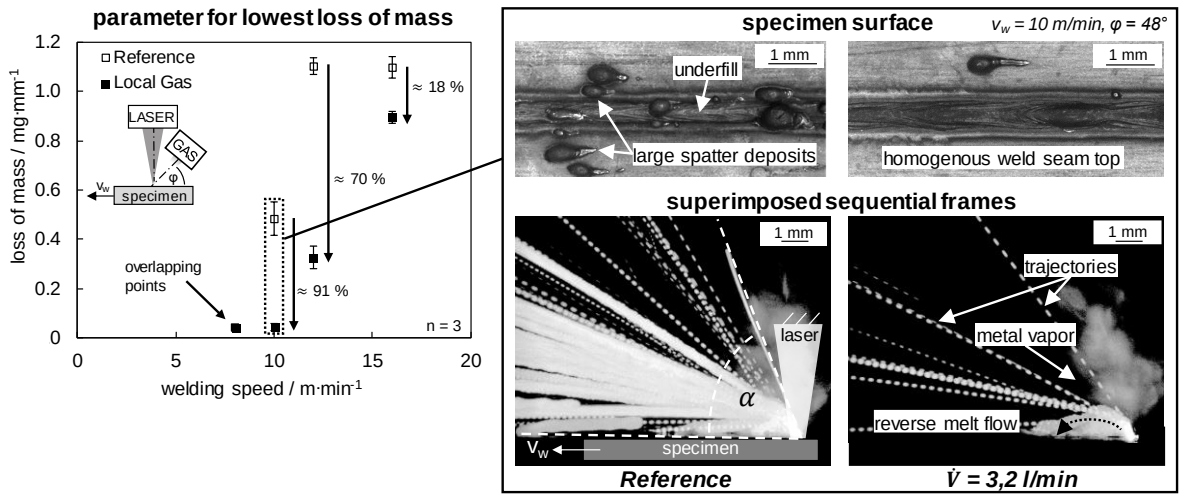

Fig.3. Loss of mass, specimen surface and superimposed sequential high-speed frames for reference process and local gas supply according to Schmidt et al., 2019

By using the local gas supply, a notable reduction in loss of mass up to 91 % at 10 m/min and by up to 70 % at 12 m/min was determined. The number of spatters adhering to the specimen surface was decreased as a result, while the formation of weld seam underfill could be avoided. Based on in-situ high-speed recordings of the specimen top side, a significant changed melt pool dynamic was observed. While the reference process was characterized by a filamentary spatter detachment on the keyhole rear wall, the local gas flow resulted in a significant stabilization of the keyhole real wall. As a result, the formation of a reverse melt flow was determined. Additionally, the local gas supply resulted in an extensive elongation of the melt pool length. To summarize the effect mechanism, it can be stated that the local gas supply has a major impact on melt pool dynamics and spatter formation. In order to clarify the mechanical interaction of the gas flow, the following section provides an estimation of the resulting pressure distribution, additionally applied to the welding process. Afterwards, the flow field characteristics for the inflow and fully developed steady-state gas supply are given.

3.2. Effect of pressure distribution

In order to estimate the applied pressure maximum of the local gas supply, the dynamic pressure of the gas p_{dyn_gas} was determined using the analytic approach of equation 2.The dynamic pressure has been additionally calculated using a numerical simulation based on a k-ω-SST multi component turbulence model (see section 2.2). The results of both approaches are given in Fig. 4 as function of flow rate using helium. In order to indicate

the deviation between the idealized analytical approach and the simulative approach considering possible turbulences, the plot also illustrates the deviation in dynamic pressure of the gas Δp_{dyn_gas}.

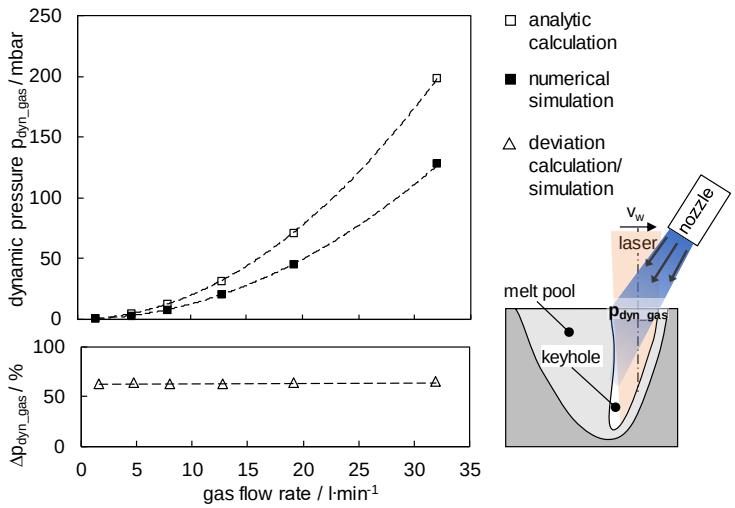

Fig.4. Dynamic pressure estimated by analytic calculation and numerical simulation

Depending on flow rate, the applied dynamic pressure Δp_{dyn_gas} increases exponentially from < 1 mbar at 1.6 l/min up to 198 mbar at 32 l/min (analytic calculation), respectively, 128 mbar at 32 l/min (numerical simulation). The pressure deviation between the two approaches is almost constant at $\Delta p_{dyn\_gas} \approx 63$ % and may be attributed to pressure loss during the inflow process of the gas (see section 3.3). According to Schmidt et al., 2019, best weld qualities were achieved by supplying argon with low flow rates up to 4.8 l/min. Neglecting the different densities of argon and helium, that implies that even a small pressure difference of ≤ 5 mbar has a significant influence on keyhole stability and spatter formation.

In order to examine the mechanical interaction of the gas more specifically, Fig. 5 shows the simulated pressure distribution of p_{dyn_gas} at flow rates of 8 l/min (Fig. 5 a) and 32 l/min (Fig. 5 b). According to Schmidt et al., 2019, these flow rates differed in their effect on melt pool dynamics and have been normalized to the dynamic pressure based on the difference in density of argon and helium.

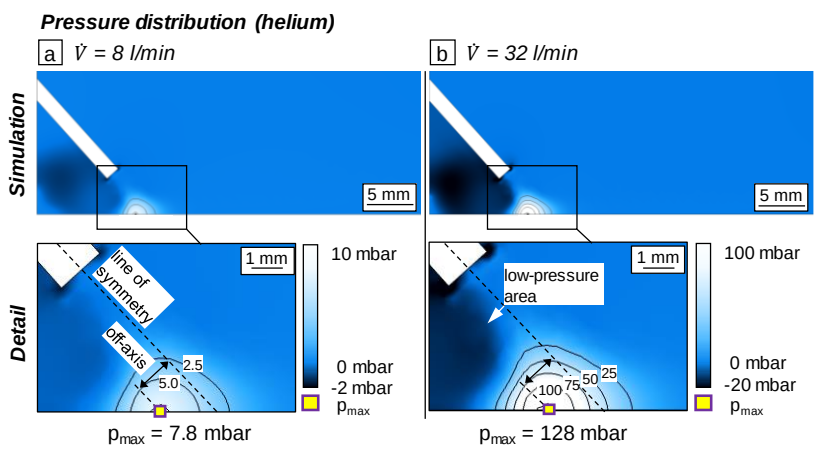

Fig.5. Simulation of pressure distribution of a local gas supply of helium at flow rates of: a) 8 l/min, b) 32 l/min

Based on the simulated pressure distribution, the interaction of the gas flow and the specimen results in a pressure increase at the specimen top side, which can be attributed to the applied dynamic pressure. The resulting pressure field spreads out in a semicircular pattern. However, the pressure maximum of 7.8 mbar at 8 l/min (Fig. 5a) and 128 mbar at 32 l/min (Fig. 5b) is not located in the line of symmetry of the nozzle. This leads to the effect that the location of pressure maximum is shifted against inflow direction. This off-axis parameter is independent of flow rate and reaches a displacement of approx. 1.2 mm. Consequently, the pressure maximum is located outside the interaction zone between the gas and the keyhole when the nozzle is aligned to the center of keyhole aperture. The area of positive pressure is followed by an area of low pressure underneath the nozzle tube. This can be attributed to the simplifications in the 2D simulation model, whereby an upwards gas transport across the nozzle tube is inhibited. Further experimental investigations will address the spatially resolved measurement of the dynamic pressure as well as a possible adjustment of the position towards the pressure maximum. To determine the effect of the local gas supply even more precisely, the following section includes the characterization of the resulting flow fields by experimental results of Schlieren videography and computational fluid dynamics analysis.

3.3. Flow field characteristics

In the following section the flow field characteristics of the supplied gas are discussed by analyzing experimental results of Schlieren videography and numerical results of CFD analysis. Therefore, the state of gas inflow as well as the fully developed steady-state were considered, in case of an idealized non-welding process. A Schlieren image velocimetry was performed using the captured Schlieren images (see section 2.1), allowing the description of gas movement based on Schlieren between local gas flow and surrounding atmosphere. This movement is represented in the following figures by vectors colored in blue.

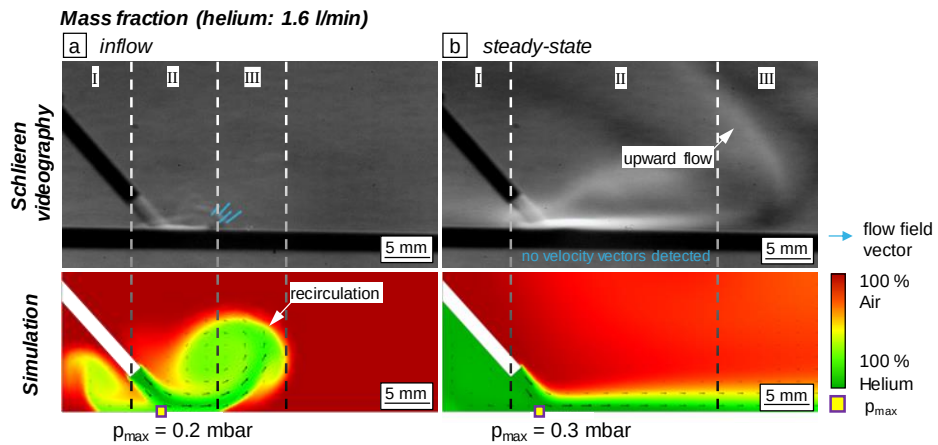

Fig.6. Flow characteristics of a helium flow of 1.6 l/min analyzed by Schlieren imaging and CFD simulation for: a) inflow, b) steady-state

In the first step, flow characteristics of helium were analyzed for the state of gas inflow at a low flow rate of 1.6 l/min (Fig. 6a). By comparing the results of Schlieren videography and CFD simulation, the flow field can be specified by three areas. While the first area (Fig. 6a, I) does not show any gas flow in the Schlieren images, the simulation indicates a forming gas accumulation underneath the nozzle. Based on the high diffusivity of helium, the time-dependent decreasing difference in density of helium and surrounding atmosphere can affect the Schlieren image contrast. This effect should be considered regarding the sensitivity of Schlieren visualization. However, this phenomenon is mainly attributed to the 2D model boundary condition, which do

not allow a gas transport throughout the nozzle tube (see section 2.2). The second area (Fig. 6a, II) is characterized by a non-separated flow that spreads parallel to specimen surface and includes the pressure maximum. With further flow propagation, the third area is reached (Fig. 6a, III). In this area, the flow is separated from the specimen top side. This phenomenon can be seen specifically in the simulative analysis, where the flow separation causes the formation of a recirculation zone. Again, the limited contrast in Schlieren images should also be taken into account regarding this effect.

In the second step, the flow characteristics of the steady-state were analyzed (Fig. 6b). According to the three-area description of the inflow-state, the steady-state is characterized by a pronounced gas accumulation in the first area of the simulative analysis (Fig. 6b, I). In contrast, no significant change in Schlieren images could be observed. The second area (Fig. 6b, II) shows a considerable enlargement of the non-separated flow, which spreads parallel to the specimen top side. While the following flow propagation in the simulative analysis shows no further changes, the Schlieren images indicate a flow separation in the third area (Fig. 6b, III). A non-swirling upward directed flow propagation was noticed. However, this flow separation has no significant effect on the welding process, since the third area is located in a far distance to the keyhole aperture (> 15 mm). Furthermore, the flow characteristics are affected by the weld seam geometry and thermal convection during the real welding process.

To be able to determine the effect of high flow rates on the flow field characteristics, the investigation was also performed for a flow rate of 30 l/min of helium (Fig.7).

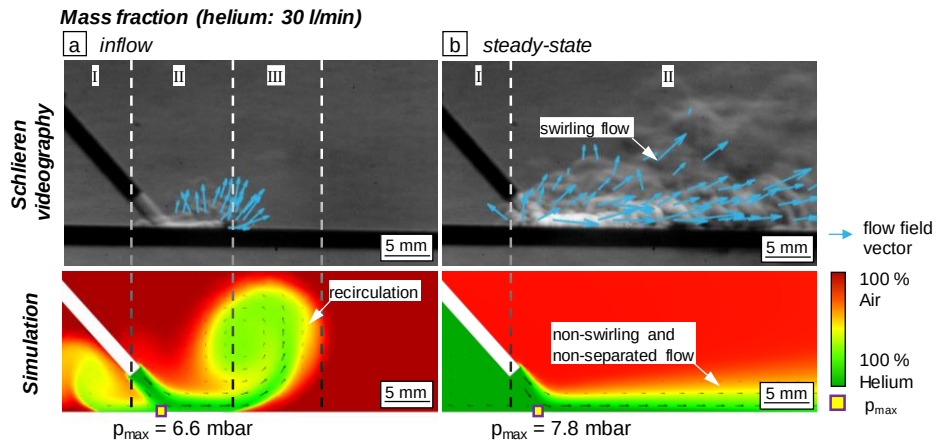

Fig.7. Flow characteristics of a helium flow of 30 l/min analyzed by Schlieren imaging and CFD simulation for: a) inflow, b) steady-state

A three-area flow field characteristic was found for the inflow process (Fig. 7a), that is similar to the characteristics of the lower flow rate of 1.6 l/min (see Fig. 6). However, the experimental and numerical results for a flow rate of 30 l/min show a much higher flow velocity of the gas. According to Zhang et al., 2011, this can result in a further acceleration of near surface melt and influence the weld seam quality. The higher flow velocities could be also seen for the steady-state gas flow (Fig. 7b). In contrast to the lower flow rate, the higher flow rate resulted in a formation of a swirling flow area (Fig. 7b, II), formed immediately after the gas flowed out of the nozzle and could only be observed by Schlieren imaging. The formation of swirls can reduce the effect of the inert shielding gas atmosphere due to the mixture with ambient atmosphere. Following, the effect of the surrounding atmosphere can be predominant regarding the surface tension-depended spatter formation and melt pool dynamics (e.g. Marangoni convection). Conversely, the simulative analysis showed a swirl-free and non-separate flow inside this area. The mismatch of experimental und numerical results can be traced back to the simplifications of the 2D simulation model, e.g. the fully developed inflow. In addition,

disturbances may present in the laboratory or production environment that are not considered in the CFD simulation, e.g. surface defects of the sheet metal or flows within the ambient atmosphere.

4. Summary

As follow-up study of Schmidt et al., 2019, this investigation characterizes the pressure field and flow field characteristics of a local gas supply of helium at different flow rates. The formed flow pattern was visualized in experiment by Schlieren videography and subsequently quantified by Schlieren image velocimetry for this purpose by using a Matlab-based image plugin (PIVlab). In correlation to the experimental investigations, the pressure field and the flow field characteristics have been analyzed by using a k-ω-SST multi component turbulence model in Comsol. Based on an analytic approach, the applied dynamic pressure of the gas flow could be approximated and correlated to the numerical results. With respect to the earlier investigations of Schmidt et al., 2019, it was shown that the best welding qualities, which were achieved by using low flow rates of ≤ 4.8 l/min, correlate to a maximum dynamic pressure of the gas flow of ≤ 5 mbar. Furthermore, it was shown, that the applied dynamic pressure spreads out unsymmetrical, which results in an off-axis position of the maximum pressure with regard to the central position of the nozzle tube. At last, it was demonstrated that the flow rate has a significant effect on the formation of the flow field. In this context, higher flow rates tend to increase the formation of flow swirls, which can significantly decrease the effect of the inert shielding gas atmosphere. The effect of the surrounding atmosphere is increasing, that can influence surface tension-driven events, e.g. spatter formation or Marangoni convection.

Further experimental investigations will address the spatially resolved measurement of the dynamic pressure and a possible adjustment of the position towards the pressure maximum.

References

Amara, E., Fabbro, R., 2008, Modelling of gas jet efect on the melt pool movements during deep penetration laser welding, in Journal of Phys. D Appl. Phys., Nr. 41, p. 055503.

Beck, M., 1996, Modellierung des Lasertiefschweißens, Universität Stuttgart, in Laser in der Materialbearbeitung.

Comsol Multiphysics 5.6, 2021, Comsol Documentation, Chemical Species Transport Interfaces: The Transport of Concentrated Species Interface.

Dreher, M., Füssel, U., Schnick, M., Hertel, M., 2009, Numerical simulation of the shielding gas flow with GMA welding and options of validation by diagnostics, International Doctoral Seminar, 17.05.2009 - 19.05.2009. Smolonice/Slowakia, p. 8

Fabbro, R., Slimani, S., Doudet, I., Coste, F., Briand, F., 2006, Experimental study of the dynamical coupling between the induced vapour plume and the melt pool for Nd–Yag CW laser welding, in Journal of Phys. D Appl. Phys., Nr. 39, p. 394–400.

Jovic, G., Bormann, A., Proell, J., Boehm, S, 2020, Laser welding with side-gas application and its impact on spatter formation and weld seam shape, in Procedia CIRP, Nr. 94, p. 649-654.

Jovic, G., Bormann, A., Proell, J., Boehm, S., 2019, Laser welding of thin stainless steel parts using modified side-gas application for control of spatter and weld shape, in Proc. Int. Congr. Laser Adv. Mater. Process, p. 1–7.

Kamimuki, K., Inoue, T., Yasuda, K., Muro, M., Nakabayashi, T., Matsunawa, A., 2002, Prevention of welding defect by side gas flow and its monitoring method in continuous wave Nd:YAG laser welding, in Journal of Laser Applications, Nr. 14, p. 136–145.

Katayama, S., Tsukamotot, S., Fabbro, R., 2013, Handbook of Laser Welding Technologies, Woodhead Publishing: Sawston, UK.

Schmidt, L., Schricker, K., Bergmann, J.P., Hickethier, S., 2019, Efect of gas flow on spatter formation in deep penetration welding at high welding speeds, in Proc. Lasers in Manuf. Conf., p. 1–7.

Schmidt, L., Schricker, K., Bergmann, J.P., Junger, C., 2020, Effect of Local Gas Flow in Full Penetration Laser Beam Welding with High Welding Speeds, in Appl. Sci., p. 1867.

Settles, G. S., 2001, Schlieren and Shadowgraph Techniques: Visualizing Phenomena in Transparent Media, Springer-Verlag Berlin Heidelberg.

Thielicke, W., 2014, The Flapping Flight of Birds - Analysis and Application, Phd thesis, Rijksuniversiteit Groningen.

Thielicke, W., Stamhuis, E., 2014, PIVlab – Towards User-friendly, Affordable and Accurate Digital Particle Image Velocimetry in MATLAB, in Journal of Open Research Software, Nr. 2(1).

Wu, D., Hua, X., Li, F., Huang, L., 2017, Understanding of spatter formation in fiber laser welding of 5083 aluminum alloy, in Int. J. Heat Mass Transf., Nr. 113, p. 730–740.

Zhang, L., Zhang, J., Zhang, G., Bo,W., Gong, S, 2011, An investigation on the efects of side assisting gas flow and metallic vapour jet on the stability of keyhole and molten pool during laser full-penetration welding, in Journal of Phys. D Appl. Phys., Nr. 44, p. 135201.